Monthly Notices
of the
ROYAL ASTRONOMICAL SOCIETY

MNRAS **467,** 731–736 (2017) doi:10.1093/mnras/stx116
Advance Access publication 2017 January 17

The length of the low-redshift standard ruler

Licia Verde,[1,2,3,4,5] José Luis Bernal,[1,6] Alan F. Heavens[7] and Raul Jimenez[1,2,3,4]★

[1]*ICC, Instituto de Ciencias del Cosmos, Universitat de Barcelona, IEEC-UB, Martí i Franquès 1, E-08028 Barcelona, Spain*
[2]*ICREA, Pg. Llus Companys 23, E-08010 Barcelona, Spain*
[3]*Radcliffe Institute for Advanced Study, Harvard University, MA 02138, USA*
[4]*Institute for Theory and Computation, Harvard–Smithsonian Center for Astrophysics, 60 Garden Street, Cambridge, MA 02138, USA*
[5]*Institute of Theoretical Astrophysics, University of Oslo, 0315 Oslo, Norway*
[6]*Departamento de Física Quàntica i Astrofísica, Universitat de Barcelona, Martí i Franquès 1, E-08028 Barcelona, Spain*
[7]*Imperial Centre for Inference and Cosmology, Imperial College, Blackett Laboratory, Prince Consort Road, London SW7 2AZ, UK*

Accepted 2017 January 13. Received 2017 January 10; in original form 2016 July 20

ABSTRACT

Assuming the existence of standard rulers, standard candles and standard clocks, requiring only the cosmological principle, a metric theory of gravity, a smooth expansion history and using state-of-the-art observations, we determine the length of the 'low-redshift standard ruler'. The data we use are a compilation of recent baryon acoustic oscillation data (relying on the standard ruler), Type Ia supernovae (as standard candles), ages of early-type galaxies (as standard clocks) and local determinations of the Hubble constant (as a local anchor of the cosmic distance scale). In a standard Λ cold dark matter cosmology, the 'low-redshift standard ruler' coincides with the sound horizon at radiation drag, which can also be determined – in a model dependent way – from cosmic microwave background observations. However, in general, the two quantities need not coincide. We obtain constraints on the length of the low-redshift standard ruler: $r_{\rm s}^h = 101.0 \pm 2.3\,h^{-1}$ Mpc, when using only Type Ia supernovae and baryon acoustic oscillations, and $r_{\rm s} = 150.0 \pm 4.7$ Mpc when using clocks to set the Hubble normalization, while $r_{\rm s} = 141.0 \pm 5.5$ Mpc when using the local Hubble constant determination (using both yields $r_{\rm s} = 143.9 \pm 3.1$ Mpc). The low-redshift determination of the standard ruler has an error, which is competitive with the model-dependent determination from cosmic microwave background measurements made with the *Planck* satellite, which assumes that it is the sound horizon at the end of baryon drag.

Key words: supernovae: general – cosmology: distance scale – large-scale structure of the Universe.

1 INTRODUCTION

We build on the idea presented in Sutherland (2012) and Heavens, Jimenez & Verde (2014) that relatively low redshift measurements of the cosmic expansion history $H(z)$ can be used, in combination with measurements of the baryon acoustic oscillation (BAO) feature, to determine the length of a standard ruler in a model-independent way. Type Ia supernovae are standard(izable) candles yielding a luminosity–distance–redshift relation. The BAO feature is probably the best-understood standard ruler in the Universe. However, it has the drawback that the comoving length of the ruler, the sound horizon at radiation drag $r_{\rm s}$, is usually calibrated at $z > 1000$ relying on cosmic microwave background (CMB) observations and theoretical assumptions. Without knowing the length of the ruler or the brightness of the candles or the Hubble parameter, these probes can give only relative measurements of the expansion history. The quantities $r_{\rm s}$ and H_0 provide absolute scales for distance measurements (anchors) at the opposite ends of the observable Universe. But while the CMB $r_{\rm s}$ determination depends on several assumptions (standard gravity, standard radiation content, negligible isocurvature perturbations, standard scaling of matter and radiation components, negligible early dark energy, etc.), local determinations of the expansion rate are cosmology-independent. Alternatively, standard clocks (Jimenez & Loeb 2002) can be used, representing objects whose age is determined by established physics, and whose formation time is sufficiently early that scatter amongst formation times is negligible in the present cosmological context. Standard clocks provide (absolute) measurements of $H(z)$.

Even relative measurements of the expansion history, from observations of Type Ia supernovae, in combination with measurements of the BAO feature, can yield a constraint on the low-redshift standard ruler, $r_{\rm s}^h$, which is the ruler length in units of h^{-1} Mpc. An *absolute* distance scale can be provided by adding a constraint on h

★ E-mail: rauljimenez@g.harvard.edu

such as that provided by H_0 or clocks, in which case observations of the BAO feature can be used to determine the absolute length of the low-redshift standard ruler, r_s, in units of Mpc. The importance of this scale is that it is a key theoretical prediction of cosmological models, depending on the sound speed and expansion rate of the Universe at early times, before matter and radiation decouple. However, the low-redshift standard ruler is a direct measurement, which will survive even if the standard cosmological model and standard assumptions about early-time physics do not. Since the analysis of Heavens et al. (2014), new BAO, H_0 and cosmic clock data have become available, with improved statistics, which we consider here.

2 DATA AND METHODOLOGY

The latest H_0 determination is provided by the SH0ES program, reaching a 2.4 per cent precision, $H_0^{\rm SH0ES} = 73.24 \pm 1.74$ km s^{-1} Mpc^{-1} (Riess et al. 2016). A Gaussian likelihood is assumed.

The Type Ia supernovae data are the compilation of Betoule et al. (2014), binned into 31 redshift intervals between 0 and 1.3, equally spaced in $\log(1+z)$ to yield the distance modulus as a function of redshift. The covariance matrix is supplied for the binned data. The binning, in conjunction with the central limit theorem, motivates the use of a Gaussian likelihood. The data are given as measurements of the distance modulus

$$\mu(z) \equiv m - M = 25 + 5\log_{10} D_{\rm L}(z), \quad (1)$$

where m is the apparent magnitude, M is a fiducial absolute magnitude, $M \simeq -19.3$, and $D_{\rm L}$ is the luminosity distance.

Constraints on the BAO are from the following galaxy surveys: Six Degree Field Galaxy Survey (Beutler et al. 2011), the LOWZ and CMASS galaxy samples of the Baryon Oscillation Spectroscopic Survey (BOSS-LOWZ and BOSS-CMASS, respectively; Cuesta et al. 2016, we use the isotropic measurement) and the reanalysed measurements of WiggleZ (Blake et al. 2011) by Kazin et al. (2014). While we take into account the correlation among the WiggleZ measurements, we neglect the correlation between WiggleZ and CMASS. This is motivated by the fact that the WiggleZ-CMASS overlap includes a small fraction of the BOSS-CMASS sample and the correlation is very small, always below 4 per cent (Beutler et al. 2016; Cuesta et al. 2016). BAO data provide measurements of the dilation scale normalized by the standard ruler length, D_V/r_s, where

$$D_V(z) \equiv \left[(1+z)^2 D_{\rm A}^2(z)\frac{cz}{H(z)}\right]^{1/3}. \quad (2)$$

If r_s is interpreted as the sound horizon at radiation drag, $r_{\rm d}(z_{\rm d})$, then

$$r_{\rm d}(z_{\rm d}) = \int_{z_d}^{\infty} \frac{c_s(z)}{H(z)}{\rm d}z, \quad (3)$$

where $c_s(z)$ is the sound speed.

Strictly speaking, the measurement of the BAO scale relies on correcting small non-linear shifts and sharpening the feature with the so-called reconstruction procedure (e.g. Noh, White & Padmanabhan 2009; Padmanabhan, White & Cohn 2009). This procedure is somewhat model-dependent (assumes Newtonian gravity), but the effect is small compared with current error bars.

For the standard clocks, we use galaxy ages determined from the analysis of stellar populations of old elliptical galaxies. We assume that the formation time was at a sufficiently high redshift that variations in formation time of stars within each galaxy and among galaxies are negligible. Differential ages, Δt, then provide estimates of the inverse Hubble parameter as $1/H(z) = {\rm d}t/{\rm d}z(1+z)$ and ${\rm d}t/{\rm d}z \simeq \Delta t/\Delta z$ for suitable redshift intervals Δz. We use the measurements of $H(z)$ obtained by Moresco et al. (2016), who extend the previously available compilation to include both a fine sampling at $0.38 < z < 0.48$ exploiting the unprecedented statistics provided by the BOSS Data Release 9 and the redshift range up to $z \sim 2$.

As in Heavens et al. (2014), we parametrize the expansion history by an inverse Hubble parameter, $\mathbf{h^{-1}}(z) \equiv 100\,{\rm km\,s^{-1}\,Mpc^{-1}}/H(z)$, which is specified at $N = 7$ values (nodes) equally spaced between $z = 0$ and 1.97; we linearly interpolate $\mathbf{h^{-1}}(z)$ in between. Since the maximum redshift probed by supernovae data is smaller than that probed by clocks, when clocks are not included, $N = 5$, and the maximum redshift value considered is $z = 1.3$. This implicitly assumes a smooth expansion history.

Assuming the cosmological principle of homogeneity and isotropy (and thus an FRW metric), the curvature of the Universe ($k = \{1, 0, -1\}$) and $H(z)$ completely specify the metric and the geometric observables considered here: luminosity distance $D_{\rm L}$ and the dilation scale D_V through the angular diameter distance $D_{\rm A}$. The curvature radius of the Universe is kR_0 (for $k = \pm 1$) and infinity for $k = 0$, where R_0 denotes the present value of the scalefactor, and the curvature is $\kappa = c/(R_0H_0)$. If we wish to further assume General Relativity (GR), the curvature density parameter is given by $\Omega_k = k[c/(R_0H_0)]^2 = k\kappa^2$ with c the speed of light.[1]

As it is customary for supernovae, we allow an absolute magnitude offset ΔM: We are assuming the existence of a standard candle, but not its luminosity. Similarly, for the BAO measurements, we assume that there is a standard ruler, which is normally interpreted as the sound horizon at radiation drag, but for the purposes here, it is simply a ruler.

The parameters are therefore (r_s^h, Ω_k, ΔM, $\mathbf{h^{-1}}(0)$, $\mathbf{h^{-1}}(z_1), \ldots, \mathbf{h^{-1}}(z_N)$). Uniform priors are assumed for all parameters. The parameter space is explored through standard Markov chain Monte Carlo (MCMC) methods.

In Section 3.1, we compare this parametrization with a prior on $H(z)$ in five knots, r_s and a spline interpolation. We also compare results for different sampling techniques: Metropolis Hastings (Hastings 1970) and Affine Invariant sampler (Goodman & Weare 2010).

3 RESULTS

In Table 1, we report the mean and 68 per cent credible regions for the recovered quantities for various combinations of the data: CSBH indicating clocks, supernovae, BAOs and local H_0, respectively. The posterior distributions are very symmetric (unless otherwise stated) and very close to Gaussian, and for this reason, herein we report symmetric error bars. However, the posterior distribution of the curvature parameter is highly non-Gaussian, except when both clocks and supernovae data are considered or in the SB case; the curvature is poorly constrained otherwise; hence, in these cases we

[1] In fact recall that

$$r(z) = \frac{c}{R_0H_0}\int_0^z \frac{{\rm d}z'}{E(z')} \equiv \frac{c}{R_0H_0}\tilde{r}(z), \quad (4)$$

where $E(z) \equiv H(z)/H_0$ and $H(z) = a^{-1}{\rm d}a/{\rm d}t$.

$$D_{\rm A}(z) = (1+z)^{-1}\frac{c}{H_0\kappa}S_k(\kappa\tilde{r}), \quad (5)$$

where $S_k(r) = \sin r$, r, $\sinh r$ for $k = 1, 0, -1$, respectively. For any metric theory of gravity, the angular diameter distance and luminosity distance are related by $D_{\rm L} = (1+z)^2 D_{\rm A}$.

Table 1. Posterior mean and standard deviation for the model parameters. In the first column, the abbreviation of the data set combination is reported: C = clocks, B = BAO, S = supernovae and H = H_0 measurement. The curvature radius of the Universe R_0 is constrained, independently of GR, but we report it in terms of the GR-specific curvature density parameter Ω_k. The curvature distribution in some cases is highly non-Gaussian; therefore, we also report in parentheses the maximum of the posterior and the 68 per cent highest posterior density interval. When supernovae are not included, ΔM is not a parameter (hence the 'N/A' table entry).

Data	$r_s^h(h^{-1}$ Mpc)	r_s(Mpc)	H_0	ΔM	$\Omega_k = k(c/H_0R_0)^2$
SBH	102.0 ± 2.5 $\left(^{+2.2}_{-2.8}\right)$	140.8 ± 4.9	72.8 ± 1.8	0.079 ± 0.083	-0.49 ± 0.64 $\left(-0.99^{+0.86}_{-0.26}\right)$
BH	107.2 ± 7.2	147 ± 10	73.0 ± 1.8	N/A	Unconstrained
SB	101.0 ± 2.3	Unconstrained	Unconstrained	Unconstrained	0.07 ± 0.61
CB	103.9 ± 5.6	149.5 ± 4.3	69.6 ± 4.2	N/A	Unconstrained
CSB	100.5 ± 1.9	150.0 ± 4.7	67.0 ± 2.5	-0.090 ± 0.079	0.36 ± 0.41
CBH	107.2 ± 3.4	148.0 ± 3.9	72.5 ± 1.7	N/A	Unconstrained
CSBH	102.3 ± 1.8	143.9 ± 3.1	71.1 ± 1.5	0.028 ± 0.047	-0.03 ± 0.31 $\left(-0.08^{+0.32}_{-0.28}\right)$
SBH	100.7 ± 1.8	138.5 ± 4.3	72.8 ± 1.8	0.083 ± 0.061	Flat
BH	107.1 ± 7.2	147 ± 10	73.0 ± 1.8	N/A	Flat
SB	101.2 ± 1.8	Unconstrained	Unconstrained	Unconstrained	Flat
CB	103.7 ± 5.5	149.8 ± 4.2	69.2 ± 4.0	N/A	Flat
CSB	101.4 ± 1.7	148.3 ± 4.3	68.5 ± 2.1	-0.047 ± 0.064	Flat
CBH	107.4 ± 3.4	148.0 ± 3.6	72.6 ± 1.7	N/A	Flat
CSBH	102.3 ± 1.6	143.9 ± 3.1	71.1 ± 1.4	0.026 ± 0.043	Flat

also report the maximum of the posterior and the 68 per cent highest posterior density interval.

The results of Table 1 indicate the following:

(1) There is only a mild dependence of the low-redshift standard ruler determination on curvature. Imposing flatness slightly reduces the error bars, and has no effect when all data sets are considered. Only in the case of SBH does imposing flatness induce a change of $\sim 1\sigma$ in the low-redshift standard ruler towards lower values.

(2) The recovered H_0 estimates cluster around two values: $h \equiv \mathbf{h}(z=0) \sim 0.73$ obtained when the local $H_0^{\rm SH0ES}$ is used (as expected); and $h \sim 0.68$ when clocks are used, and 0.71 when both are used.

(3) These two values for H_0 correspond to the low versus high Hubble constant obtained, respectively, from the *Planck* CMB analysis assuming a Λcolddarkmatter(ΛCDM) model and the local measurement based on cepheids and local supernovae (Riess et al. 2016). A more detailed discussion and extended analysis can be found in Bernal, Verde & Riess (2016, hereafter BVR).

(4) The H_0 value obtained by the CSB combination has an error bar of 3.7 per cent, to be compared with a 2.4 per cent error for $H_0^{\rm SH0ES}$ and a 3.8 per cent error for H0LiCOW (Bonvin et al. 2016). These two measurements are in agreement at the 2σ level with the CSB value.

(5) Supernovae and cosmic clocks data are needed to constrain the curvature. The curvature distribution is highly non-Gaussian, unless these data sets are considered.

(6) Without $H_0^{\rm SH0ES}$, $r_{\rm s}$ tends to be ∼149 Mpc, as expected, and $H_0^{\rm SH0ES}$ pulls the recovered $r_{\rm s}$ downwards.

(7) Depending on how extensive the data set considered is, the error on $r_{\rm s}^h$ varies between 7 per cent (for BH) to 1.8 per cent (CSBH), and the error on $r_{\rm s}$ varies between 7 per cent (for BH) to 2.1 per cent (CSBH).

(8) While $r_{\rm s}^h$ is better determined than $r_{\rm s}$, the recovered value across different data sets is more consistent for $r_{\rm s}$.

(9) $r_{\rm s}^h$ is determined at the 2 per cent level with only BAOs and supernovae. In this case, the curvature distribution is remarkably more symmetric than for the SBH case.

Fig. 1 offers visual comparisons of the $r_{\rm s}^h$ and $r_{\rm s}$ measurements, for the flat case and marginalizing over curvature. The CSB combination yields an $r_{\rm s}$ value fully consistent with the *Planck* mission CMB inferred one, while the SBH determination yields lower values, which are still consistent in the non-flat case but become an $\sim 2\sigma$ tension (with respect to the *Planck* value for the ΛCDM model) when flatness is imposed.

Fig. 2 shows the envelope enclosing 95 per cent of the reconstructed $H(z)$ for two representative data set combinations. The odd shape of the envelope is due to the fact that the linear interpolation is being performed in $1/H$, while the quantity plotted is $H(z)$. Symbols represent the best-fitting $H(z)$ of each redshift. The highest redshift nodes are poorly constrained and therefore not shown. Also for the CSBH case, the joint distribution of the $\mathbf{h^{-1}}(z_n)$ values for the last two redshift nodes shows a structure indicating a high degree of interdependence between the two quantities. This does not affect the determination of the standard ruler, as there is no correlation between $r_{\rm s}$ or $r_{\rm s}^h$ and $\mathbf{h^{-1}}(z_n)$ for $n \geq 4$.

3.1 Robustness to prior assumptions

To assess the dependence on the prior assumptions, we compare our findings with the results and the approach of BVR. In that work, a similar reconstruction of the late time expansion history is performed in the context of the study of the tension between the (direct) local H_0 determination and its CMB-inferred value within the ΛCDM model. However, they use a different parametrization and sampling method: $H(z)$ and $r_{\rm s}$ are the free parameters, and $H(z)$ values are interpolated using natural cubic splines, instead of $r_{\rm s}^h$, $\mathbf{h^{-1}}(z)$ and linear interpolation as done here. They also use an Affine Invariant sampler [implemented in the public code EMCEE (Foreman-Mackey et al. 2013)] instead of Metropolis Hastings. BVR do not include cosmic clocks, so we concentrate on the SBH data combination for this test. The number of nodes is the same ($N = 5$), although their location is different. We isolate each of the methodological differences to study their effect in the final results.

As supernovae data impose very strong constraints on the shape of $H(z)$, the resulting expansion history does not depend on the

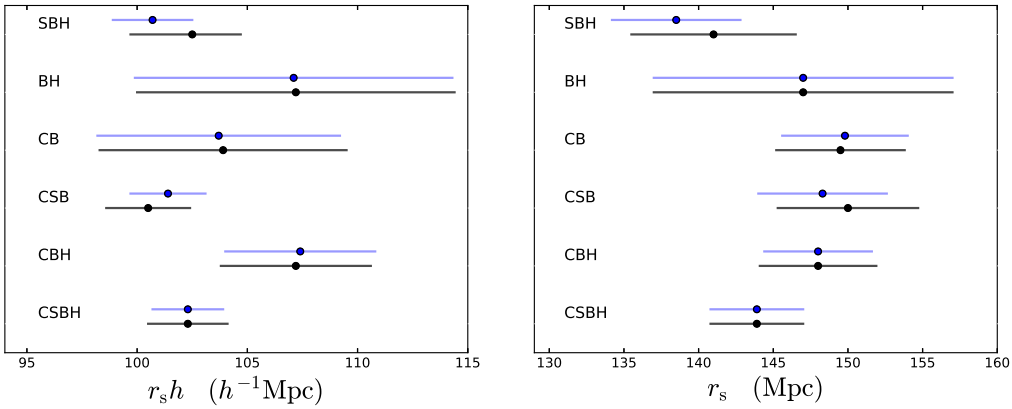

Figure 1. At a glance: comparison of central values and 1σ errors on the r_s^h (left-hand panel) and r_s (right-hand panel) measurements for flat geometry (blue) and marginalizing over the curvature (black). Note the change of the scale in the x-axis in each figure.

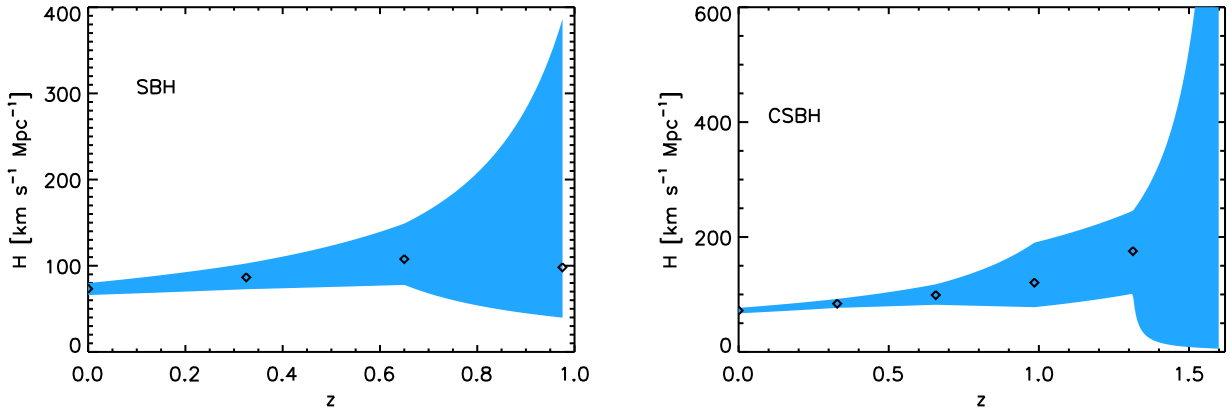

Figure 2. Reconstructed expansion history $H(z)$ (95 per cent confidence envelop) for two representative data set combinations: SBH (left-hand panel) CSBH (right-hand panel). The last redshift nodes (one on the left-hand side, two on the right-hand side) are not shown as there $H(z)$ is poorly constrained. The jagged shape of the envelop is due to the linear interpolation being performed in $1/H$, while the quantity plotted is $H(z)$. Symbols represent the best-fitting values for the reconstruction.

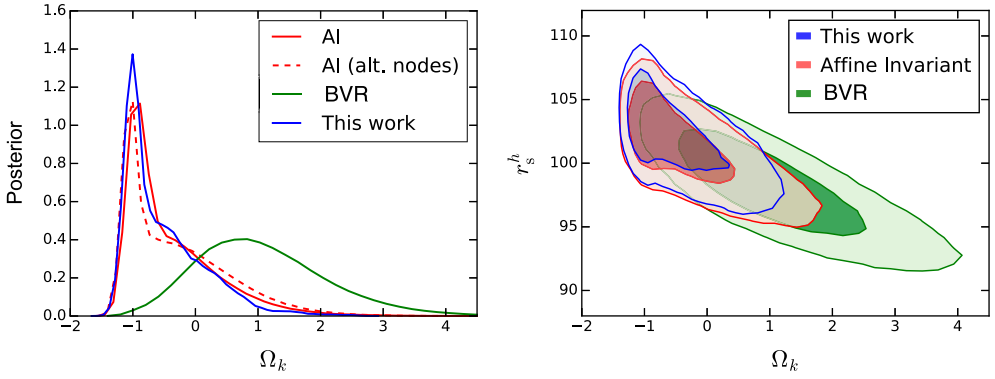

Figure 3. Effects of prior assumptions and the MCMC sampling method. We show the comparison of the posterior distributions of Ω_k (left-hand panel) and in the Ω_k–r_s^h plane (right-hand panel) obtained from the same data (SBH) with different methodologies: this work (blue), using an Affine Invariant sampler instead of Metropolis Hastings (red) with two choices for the redshift sampling, the one from this work (solid) and the other from BVR (dashed), and the approach of BVR (green), which uses an Affine Invariant sampler, r_s and $H(z_i)$ as variables and a spline interpolation of $H(z)$.

interpolation method, even taking into account that the splines allow much more freedom than the linear interpolation. Also, the location of the knots does not have any significant effect in the final fit of the reconstruction. It does, however, have a mild effect on the curvature, which is the parameter most weakly constrained.

In Fig. 3, we show the posterior distribution of Ω_k (left-hand panel) and the joint distribution in the Ω_k–r_s^h plane (right-hand panel) for the different cases compared in this section. The distributions are marginalized over all other parameters. We refer as 'Affine Invariant' to the case when the only change with respect to this work is the MCMC sampler. The figure also quantifies the effect of a different choice of redshift sampling (nodes). Unlike in our parametrization, using r_s and $H(z)$ as free parameters makes the distribution of Ω_k

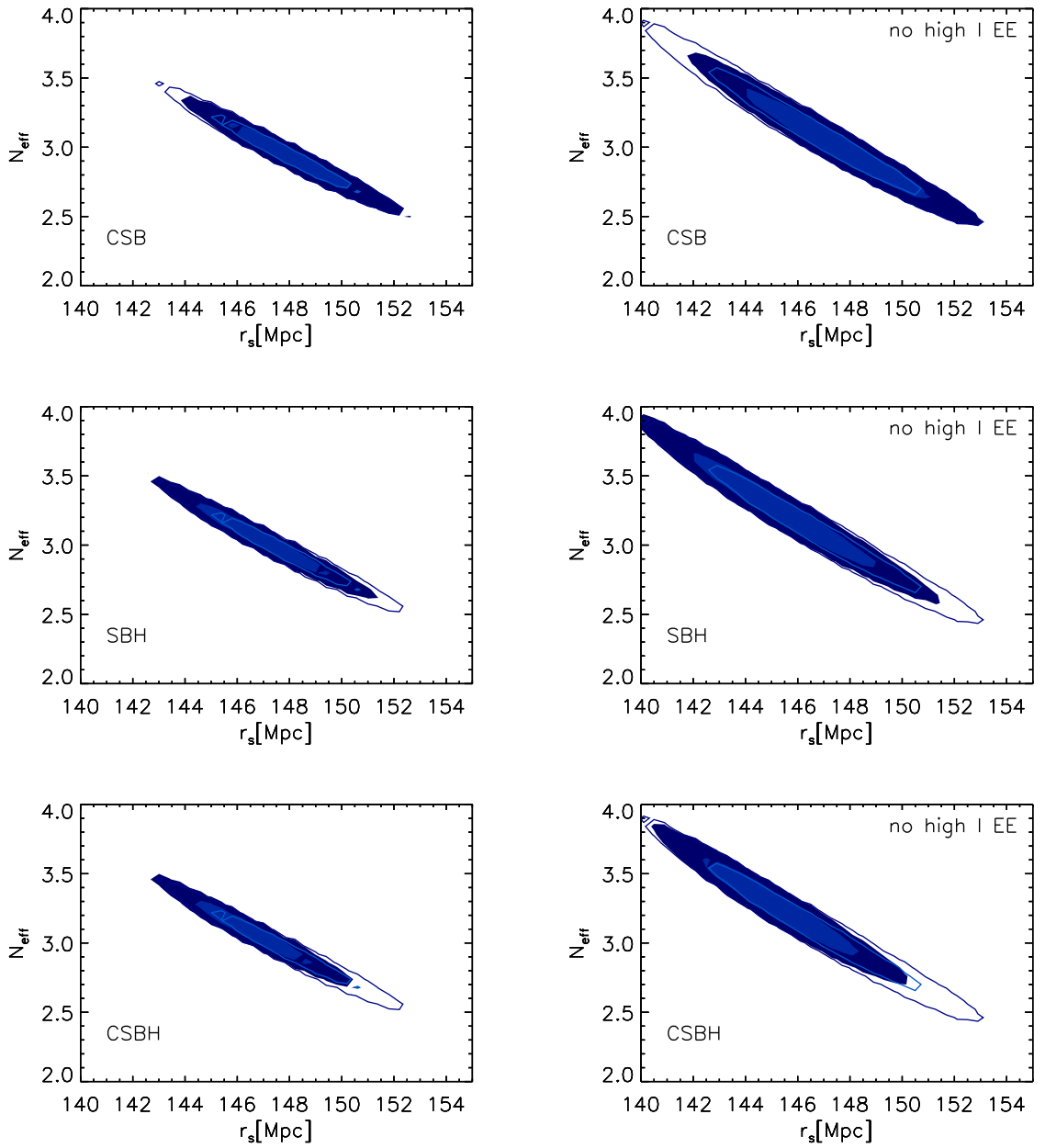

Figure 4. Effect of combining the low-redshift standard ruler measurement (interpreted as the sound horizon at radiation drag) with *Planck* CMB observations. The transparent contours show the joint r_s versus N_{eff} 68 per cent and 95 per cent marginalized confidence regions obtained from the posterior sample provided by the *Planck* CMB mission. On the left-hand side, all temperature and polarization data are used, whereas on the right-hand side, high-ℓ polarization data are not included. The filled contours result from importance sampling this with our CSB measurement (top row), SBH (middle row) and CSBH (bottom row).

Gaussian, but centred around higher values and with larger error bars.

As r_s and Ω_k are anticorrelated (and Ω_k and H_0 are independent), differences in the posterior of Ω_k result in different determinations of the low-redshift standard ruler. The values of r_s and r_s^h obtained in this work (for the non-flat case) are $\sim 1\sigma$ higher than in BVR. Once flatness is imposed, the discrepancies between the two sampling algorithms and prior choices disappear.

It is important to point out that the dependence of the posterior on the prior choice and the MCMC sampling method appears only when the parameters are weakly constrained. This is the case when using only BAOs, supernovae and H_0 (SBH) and not imposing flatness. Both cosmic clocks and supernovae data are needed to obtain a Gaussian posterior distribution for the curvature: In these cases (CSBH and CSB), the dependence on the prior assumptions and the sampler becomes unimportant. The dependence on prior is negligible also for the SBH data set combination when flatness is imposed.

4 DISCUSSION AND CONCLUSIONS

This model-independent determination of the low-redshift standard ruler can be interpreted as the sound horizon at the baryon drag and thus compared with (model-dependent) CMB determinations. This comparison can be used to limit the scope of new physics that may alter the early expansion rate and sound speed. This is investigated in detail, for example, in Bernal et al. (2016). Here, we only compare our constraints with those obtained by the Planck team with the

Planck 2015 data release, using publicly available posterior samples (Planck Collaboration XIII 2015). The direct measurement of the ruler is in good agreement with the CMB-derived one for all models considered by the Planck team and especially the standard ΛCDM model. In all cases, the CMB-inferred error bars are, understandably, much smaller, with one notable exception: the model where the effective number of neutrino species is free (Heavens et al. 2014). The effect of combining our measurement with the CMB one is illustrated in Fig. 4. Transparent contours are the (joint) 68 per cent and 95 per cent confidence regions for CMB data alone, including (excluding) high-ℓ polarization data on the left-hand (right-hand) panel. The filled contours result from importance sampling this with our SBH, CSB or CSBH measurement, which reduces the errors significantly. When $H_0^{\rm SH0ES}$ is included, the error on $N_{\rm eff}$ is reduced by suppressing the posterior for low $N_{\rm eff}$ values. A similar trend was found by Riess et al. (2016) and by BVR.

Note that even without an estimate of h, the combination of BAO and supernovae data already constrains the low-redshift standard ruler scale $r_{\rm s}^h$ at the 2 per cent level, $r_{\rm s}^h = 101.0 \pm 2.3$ Mpc h^{-1}.

Looking ahead, improvements on the low-redshift standard ruler measurement may arise from the next generation of BAO surveys. For example, if in the CSB (or CSBH) combination we substitute the current BAO measurements with forecasted constraints achievable with a survey with the specifications of DESI (Levi et al. 2013), errors without imposing flatness will reduce as follows. The error on $r_{\rm s}^h$ will go from 1.9 per cent to 1.3 per cent (1.8 per cent to 1.1 per cent), the error on $r_{\rm s}$ from 3.2 per cent to 2.8 per cent (2.2 per cent to 1.9 per cent), the error on H_0 from 3.7 per cent to 3.4 per cent (2.1 per cent to 2 per cent) and the error on Ω_k from ± 0.41 to ± 0.28 (± 0.31 to ± 0.22). For the SB combination, we find an error on $r_{\rm s}^h$ of 1.5 per cent, and 1.3 per cent with flatness imposed. Given the dramatic improvement in the precision of expansion history constraints provided by the next generation of BAO surveys, these forecasts indicate that we are entering a regime where the error on $r_{\rm s}^h$ is dominated by the supernovae errors and the error on $r_{\rm s}$ is dominated by that on the normalization of the expansion history h, and therefore directly or indirectly on H_0. Improvement on the local H_0 determination towards a goal of $\sim$1 per cent error budget may be provided by, for example, gravitational lensing time delays (Suyu et al. 2016) and by further improvements of the classic distance ladder approach (Riess et al. 2016).

ACKNOWLEDGEMENTS

LV and JLB thank A. Riess for discussions. RJ and LV acknowledge support from Mineco grants AYA2014-58747-P and MDM-2014-0369 of ICCUB (Unidad de Excelencia Maria de Maeztu), and a visiting scientist grant from the Royal Society. JLB is supported by the Spanish MINECO under grant BES-2015-071307, co-funded by the ESF. JLB and AFH acknowledge the hospitality of the Radcliffe Institute for Advanced Study, Harvard University. AFH, RJ and LV acknowledge the Imperial College for support under the CosmoCLASSIC collaboration.

Based on observations obtained with *Planck* (http://www.esa.int/Planck), an ESA science mission with instruments and contributions directly funded by ESA Member States, NASA and Canada.

Funding for SDSS-III has been provided by the Alfred P. Sloan Foundation, the Participating Institutions, the National Science Foundation, and the US Department of Energy Office of Science. The SDSS-III web site is http://www.sdss3.org/.

SDSS-III is managed by the Astrophysical Research Consortium for the Participating Institutions of the SDSS-III Collaboration including the University of Arizona, the Brazilian Participation Group, Brookhaven National Laboratory, Carnegie Mellon University, University of Florida, the French Participation Group, the German Participation Group, Harvard University, the Instituto de Astrofisica de Canarias, the Michigan State/Notre Dame/JINA Participation Group, Johns Hopkins University, Lawrence Berkeley National Laboratory, Max Planck Institute for Astrophysics, Max Planck Institute for Extraterrestrial Physics, New Mexico State University, New York University, Ohio State University, Pennsylvania State University, University of Portsmouth, Princeton University, the Spanish Participation Group, University of Tokyo, University of Utah, Vanderbilt University, University of Virginia, University of Washington and Yale University.

REFERENCES

Bernal J. L., Verde L., Riess A. G., 2016, JCAP, 10, 019, (BVR)
Betoule M. et al., 2014, A&A, 568, A22
Beutler F. et al., 2011, MNRAS, 416, 3017
Beutler F., Blake C., Koda J., Marín F. A., Seo H.-J., Cuesta A. J., Schneider D. P., 2016, MNRAS, 455, 3230
Blake C. et al., 2011, MNRAS, 418, 1707
Bonvin V. et al., 2016, MNRAS, 465, 4914
Cuesta A. J. et al., 2016, MNRAS, 457, 1770
Foreman-Mackey D., Hogg D. W., Lang D., Goodman J., 2013, PASP, 125, 306
Goodman J., Weare J., 2010, Comm. App. Math. Comp., 5, 65
Hastings W. K., 1970, Biometrika, 57, 97
Heavens A., Jimenez R., Verde L., 2014, Phys. Rev. Lett., 113, 241302
Jimenez R., Loeb A., 2002, ApJ, 573, 37
Kazin E. A. et al., 2014, MNRAS, 441, 3524
Levi M. et al., 2013, preprint (arXiv:1308.0847)
Moresco M. et al., 2016, J. Cosmol. Astropart. Phys., 5, 014
Noh Y., White M., Padmanabhan N., 2009, Phys. Rev. D, 80, 123501
Padmanabhan N., White M., Cohn J. D., 2009, Phys. Rev. D, 79, 063523
Planck Collaboration XIII, 2015, A&A, 594, A13
Riess A. G. et al., 2016, AJ, 826, 56
Sutherland W., 2012, MNRAS, 426, 1280
Suyu S. H. et al., 2016, MNRAS, preprint (arXiv:1607.00017)

This paper has been typeset from a TEX/LATEX file prepared by the author.